Supporting information for:

Reactivity of an Unsaturated Iridium(III) Phosphoramidate Complex, [Cp*Ir{κ^2-*N*,*O*}][BAr$^F{}_4$]

Marcus W. Drover,[a,b] Heather C. Johnson,[b] Laurel L. Schafer,[a] Jennifer A. Love,[a] and Andrew S. Weller*[,b]

[a]Department of Chemistry, The University of British Columbia, 2036 Main Mall, Vancouver, British Columbia, Canada V6T 1Z1

[b]Department of Chemistry, The University of Oxford, Chemistry Research Laboratories, Mansfield Road, Oxford, U.K. OX1 3TA

**e-mail: andrew.weller@chem.ox.ac.uk*

Figure S1. [1], ^{1}H NMR, CD_2Cl_2, 400 MHz, 298 K

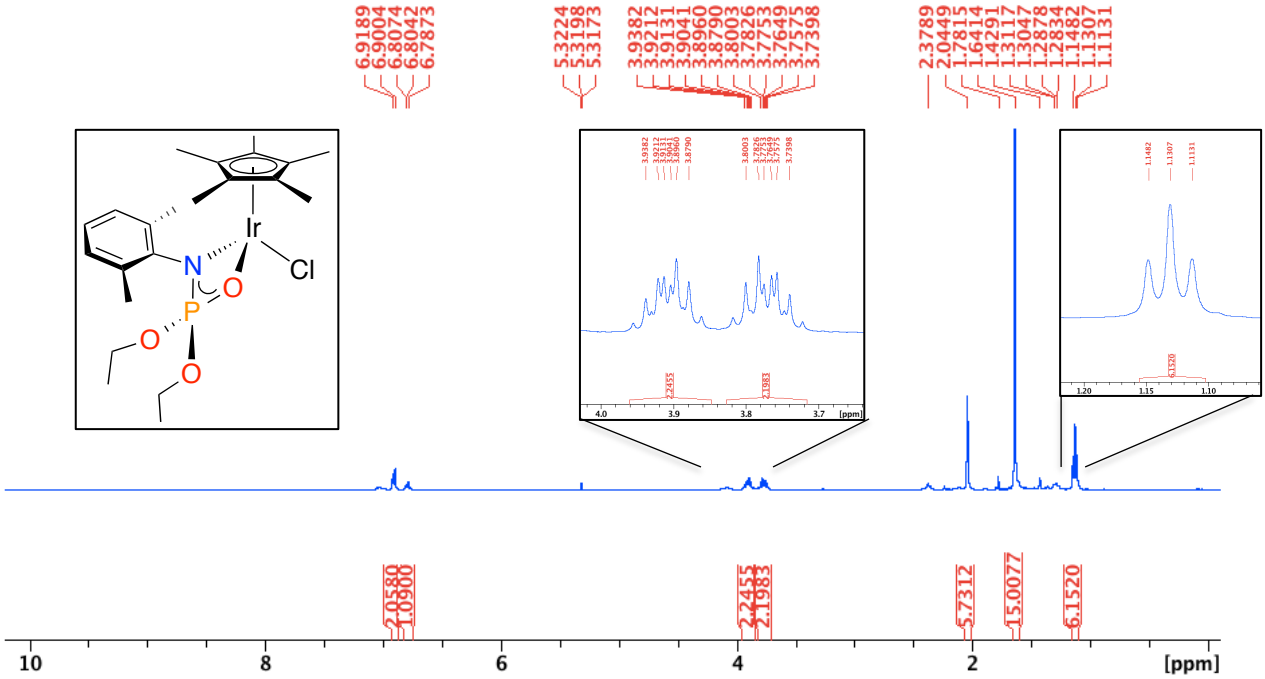

Figure S2. [1], $^{31}P\{^{1}H\}$ NMR, CD_2Cl_2, 121 MHz, 298 K

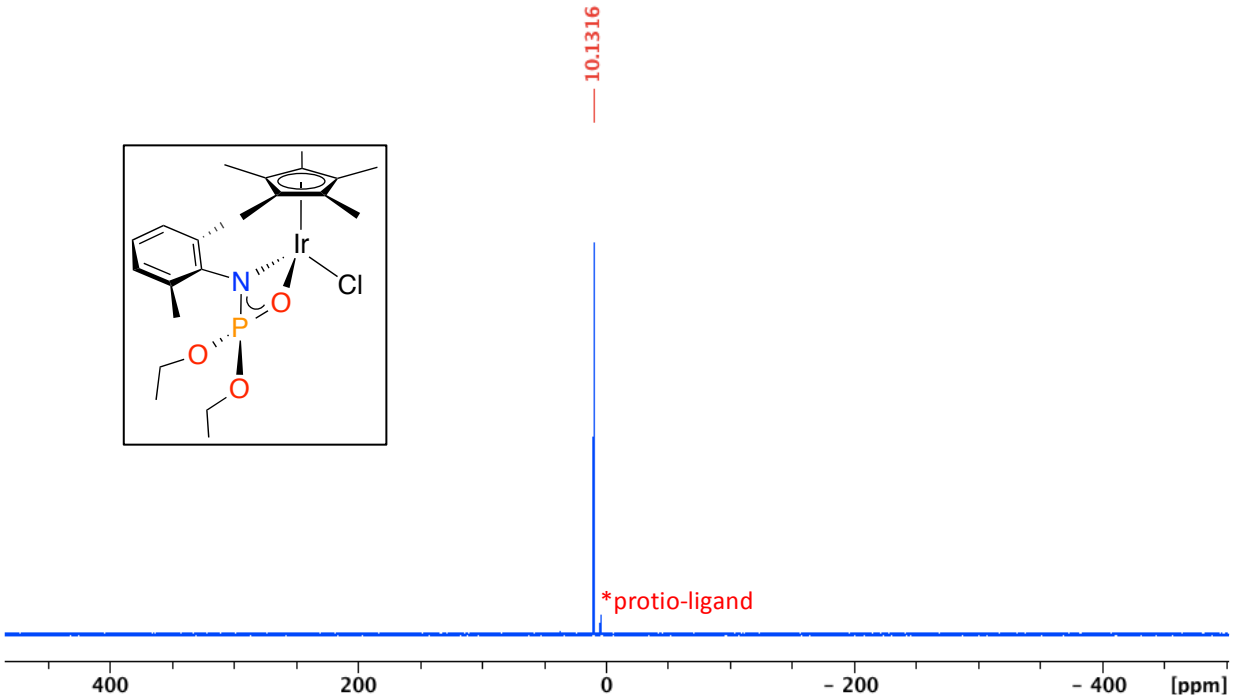

Figure S3. [1], $^{13}C\{^{1}H\}$ NMR, $CDCl_3$, 100 MHz, 298 K

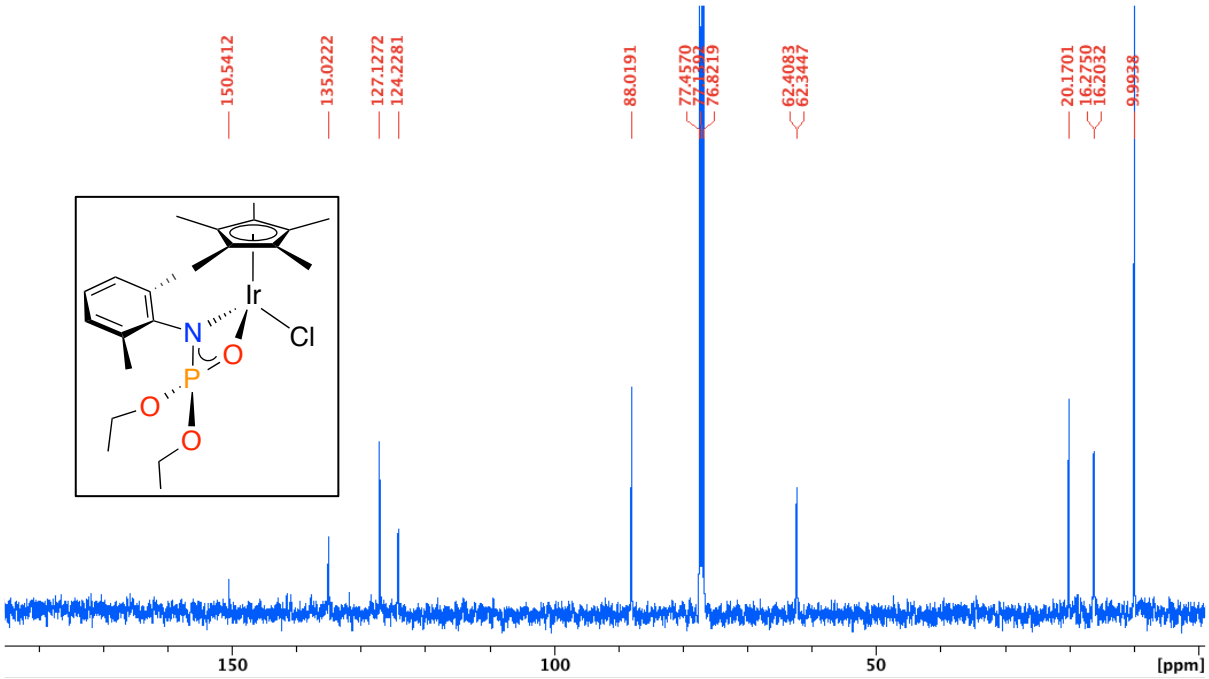

Figure S4. [2][BAr$^{F}_{4}$], ^{1}H NMR, CD_2Cl_2, 400 MHz, 298 K

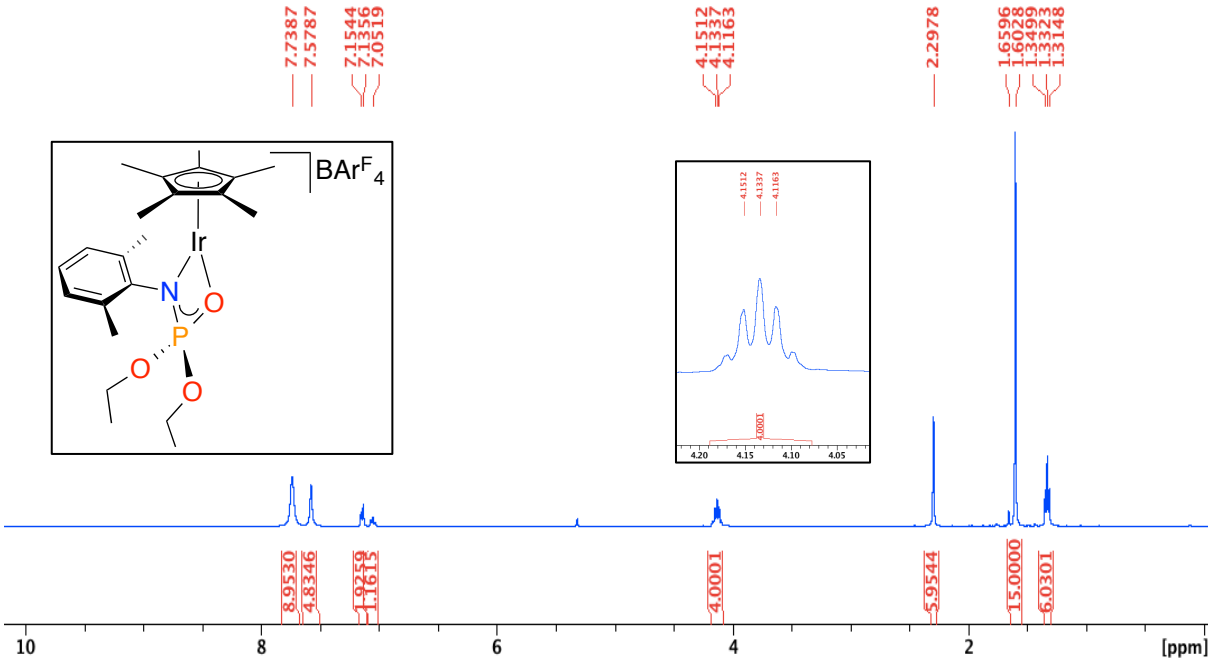

Figure S5. [2][BAr$^F_4$], $^{31}P\{^1H\}$ NMR, CD_2Cl_2, 121 MHz, 298 K

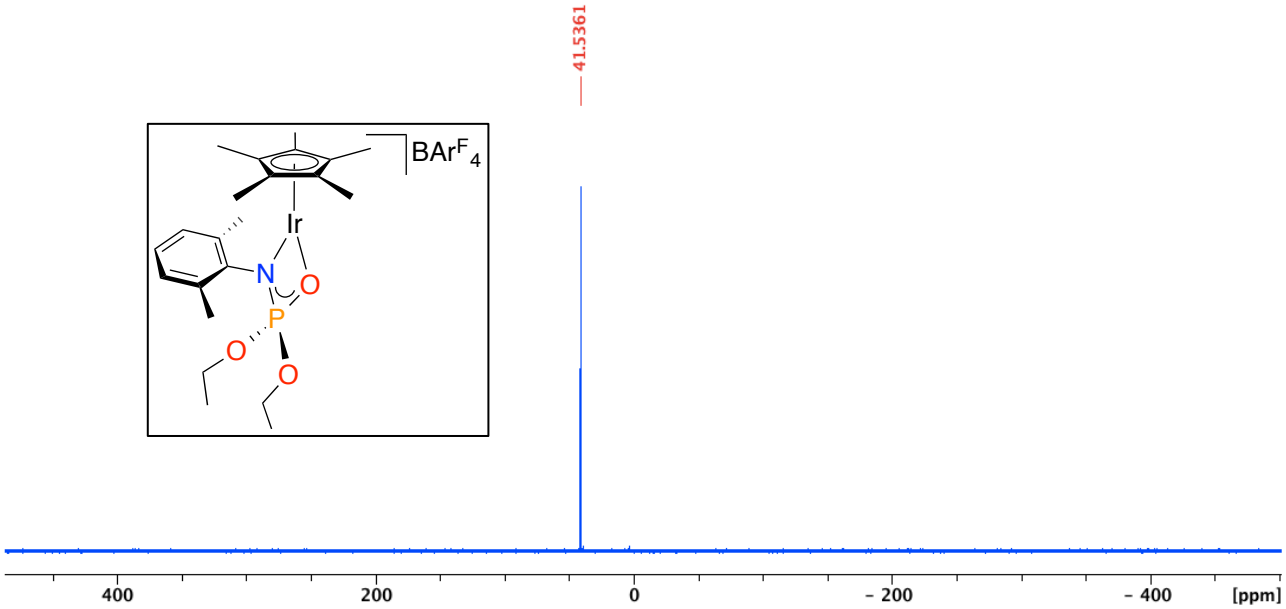

Figure S6. [2][BAr$^F_4$], $^{13}C\{^1H\}$ NMR, CD_2Cl_2, 100 MHz, 298 K

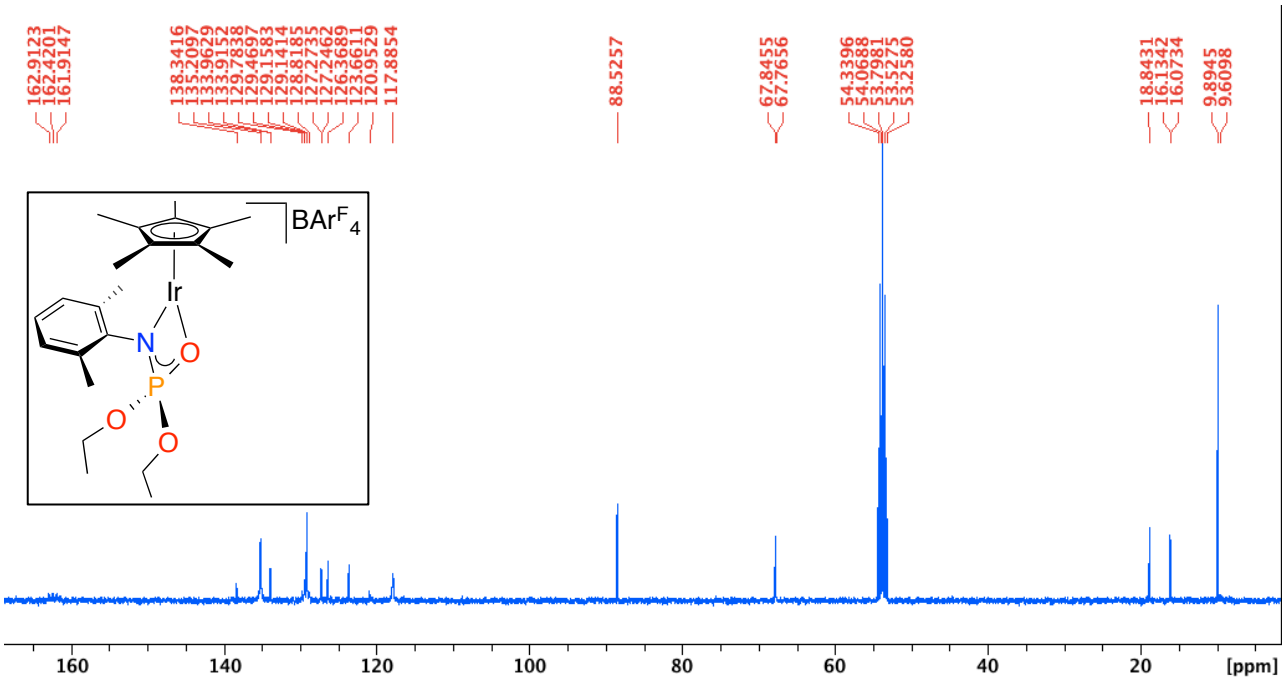

Figure S7. [2][BAr$^F_4$], ESI(+)-MS

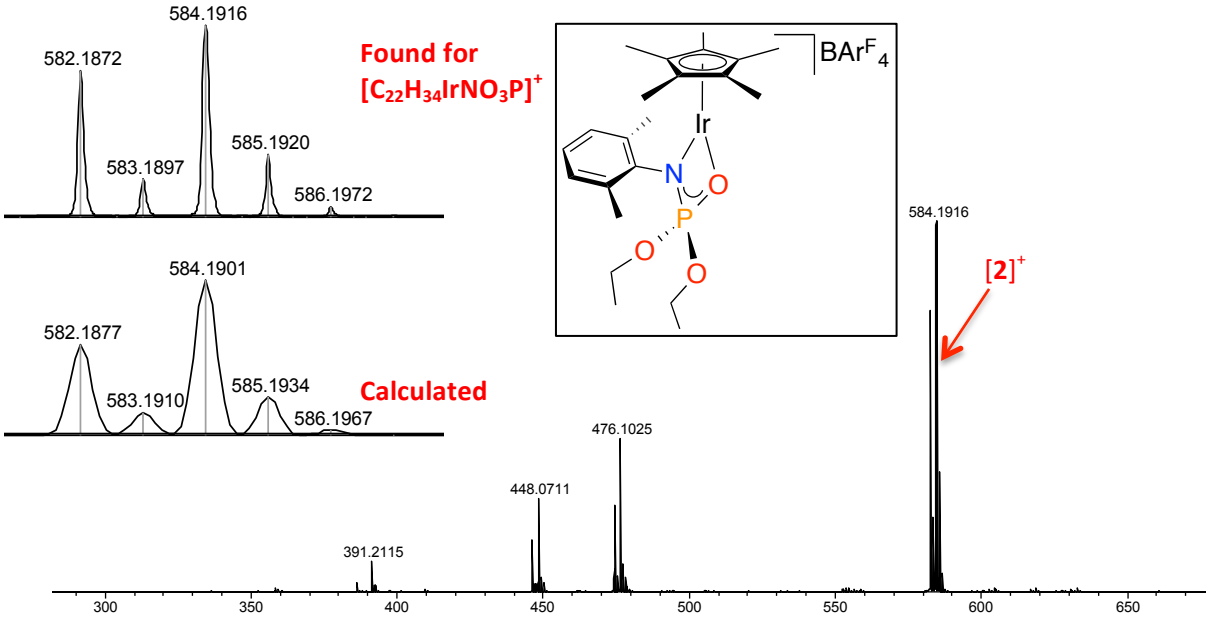

Figure S8. [3][BAr$^F_4$], ^{1}H NMR, $CDCl_3$, 400 MHz, 298 K

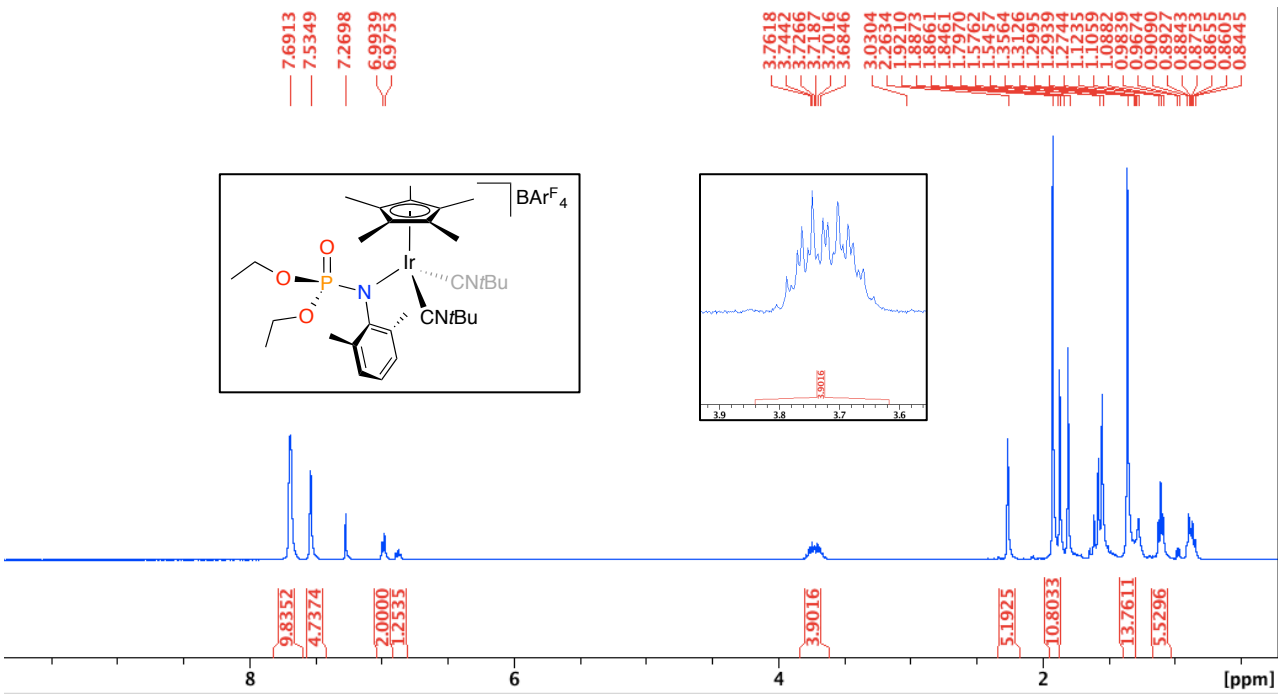

Figure S9. [3][BAr$^F_4$], $^{31}P\{^1H\}$ NMR, CD_2Cl_2, 121 MHz, 298 K

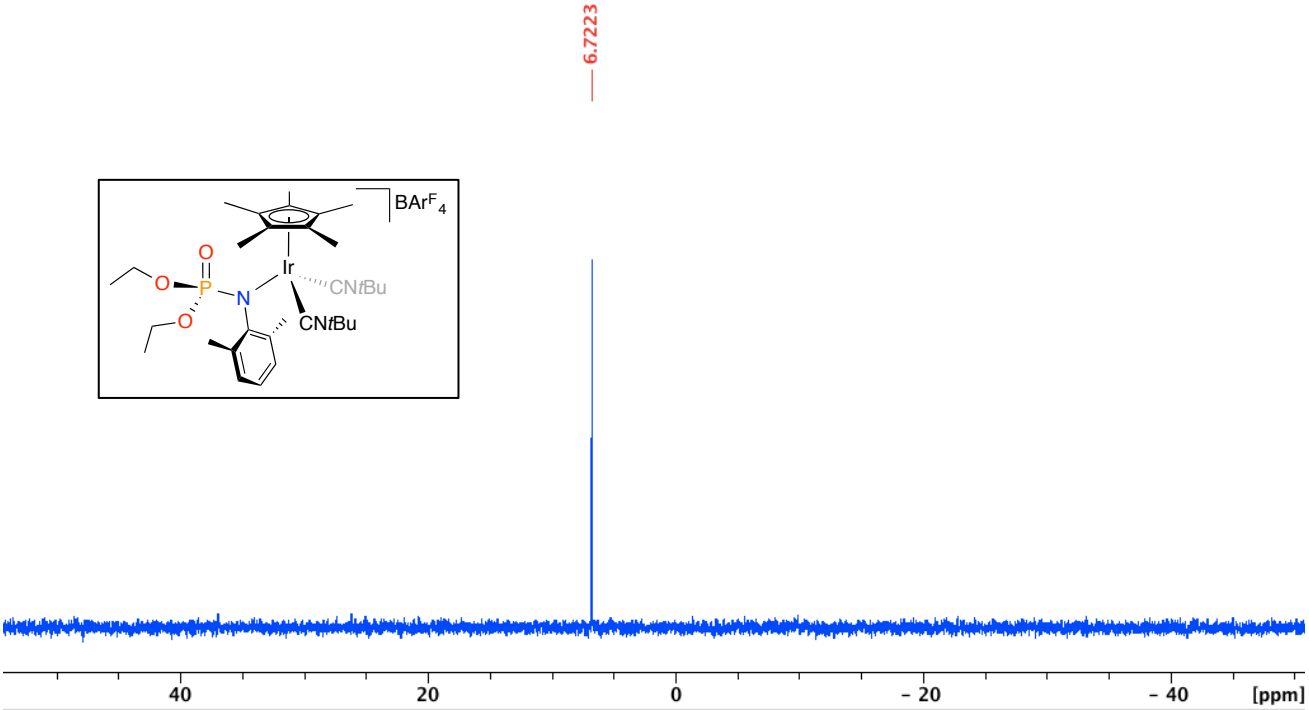

Figure S10. [3][BAr$^F_4$], $^{13}C\{^1H\}$ NMR, CD_2Cl_2, 100 MHz, 298 K

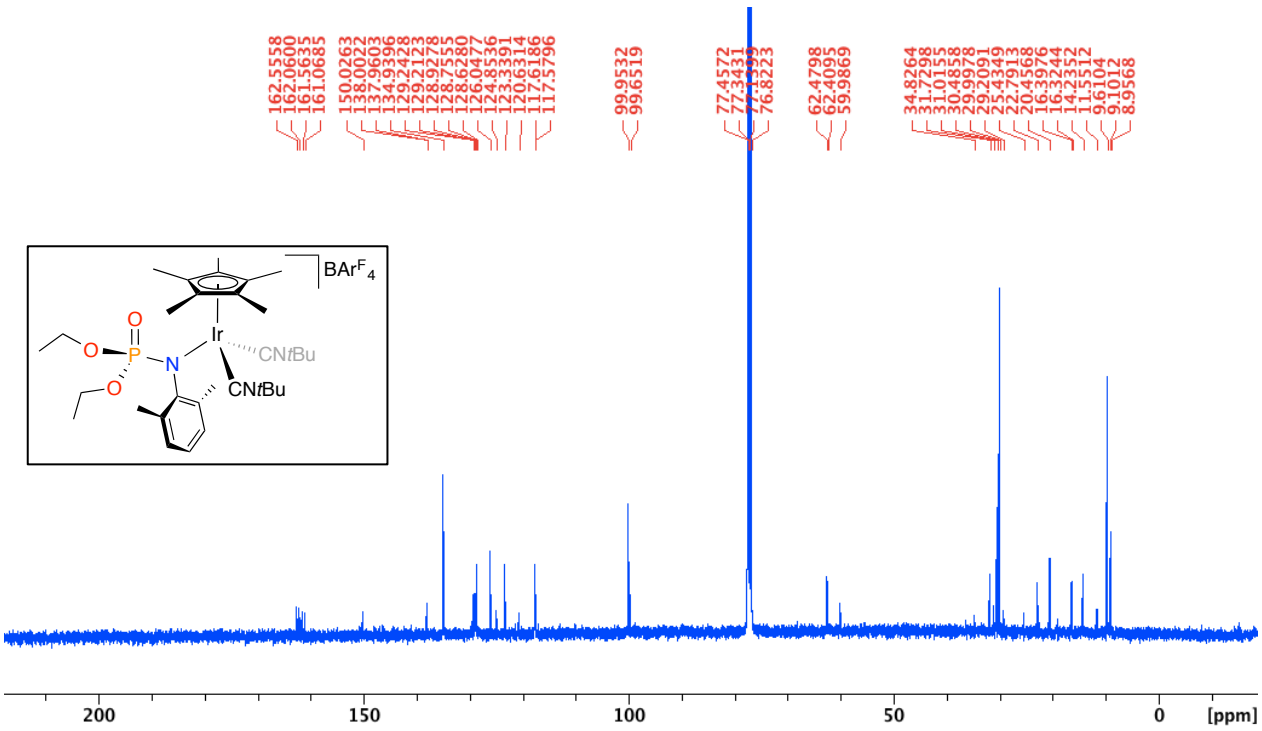

Figure S11. [3][BAr$^F_4$], ESI(+)-MS

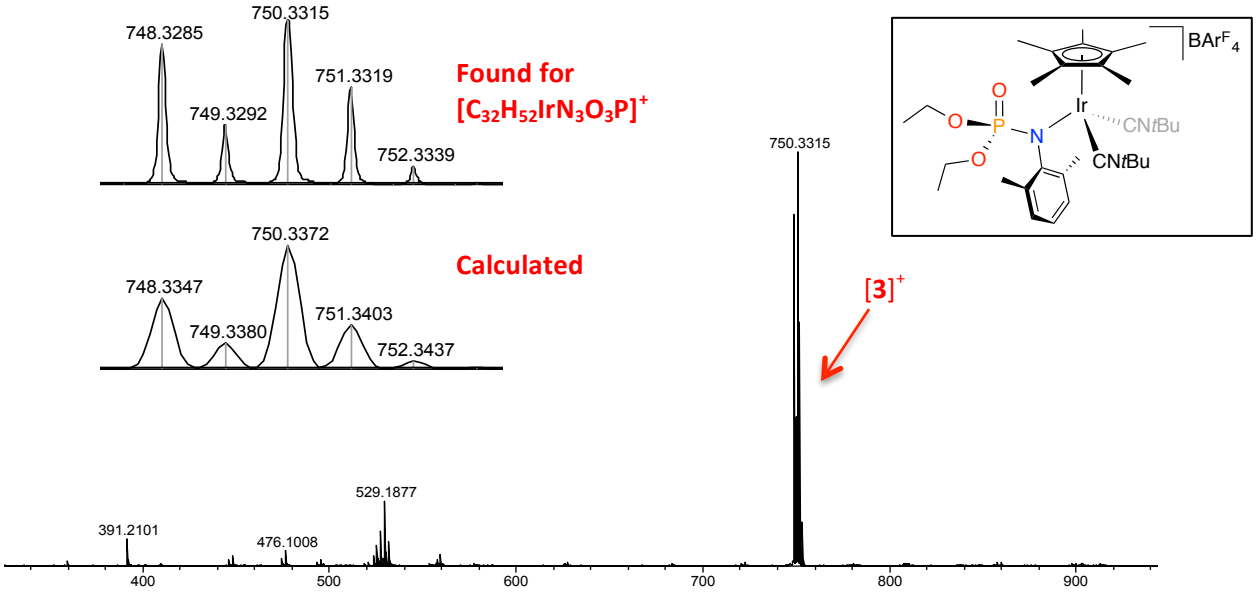

Figure S12. [4][BAr$^F_4$], ^{1}H NMR, CD_2Cl_2, 400 MHz, 298 K

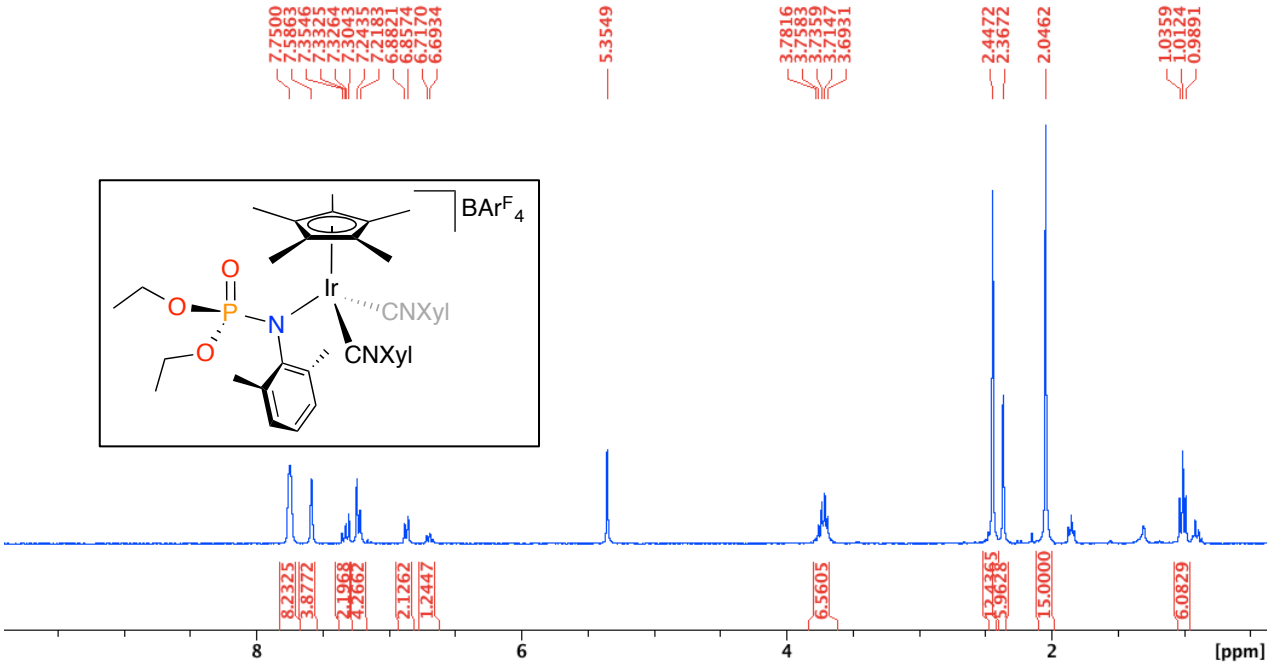

Figure S13. [4][BAr$^F_4$], $^{31}P\{^1H\}$ NMR, CD_2Cl_2, 121 MHz, 298 K

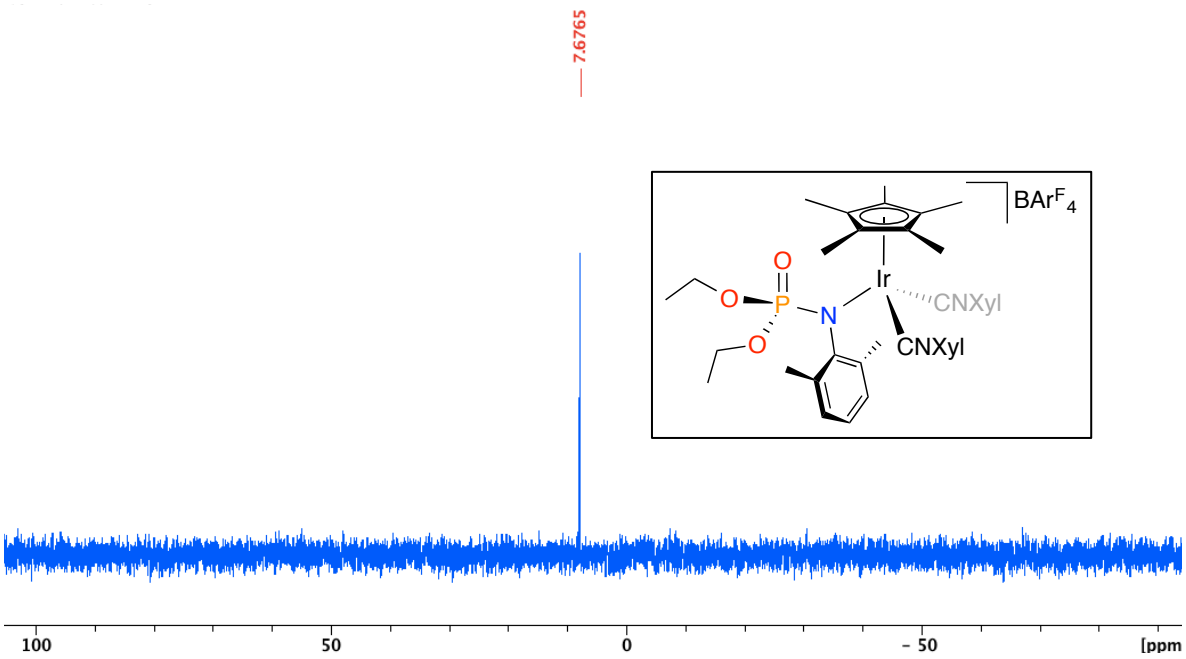

Figure S14. [4][BAr$^F_4$], $^{13}C\{^1H\}$ NMR, CD_2Cl_2, 100 MHz, 298 K

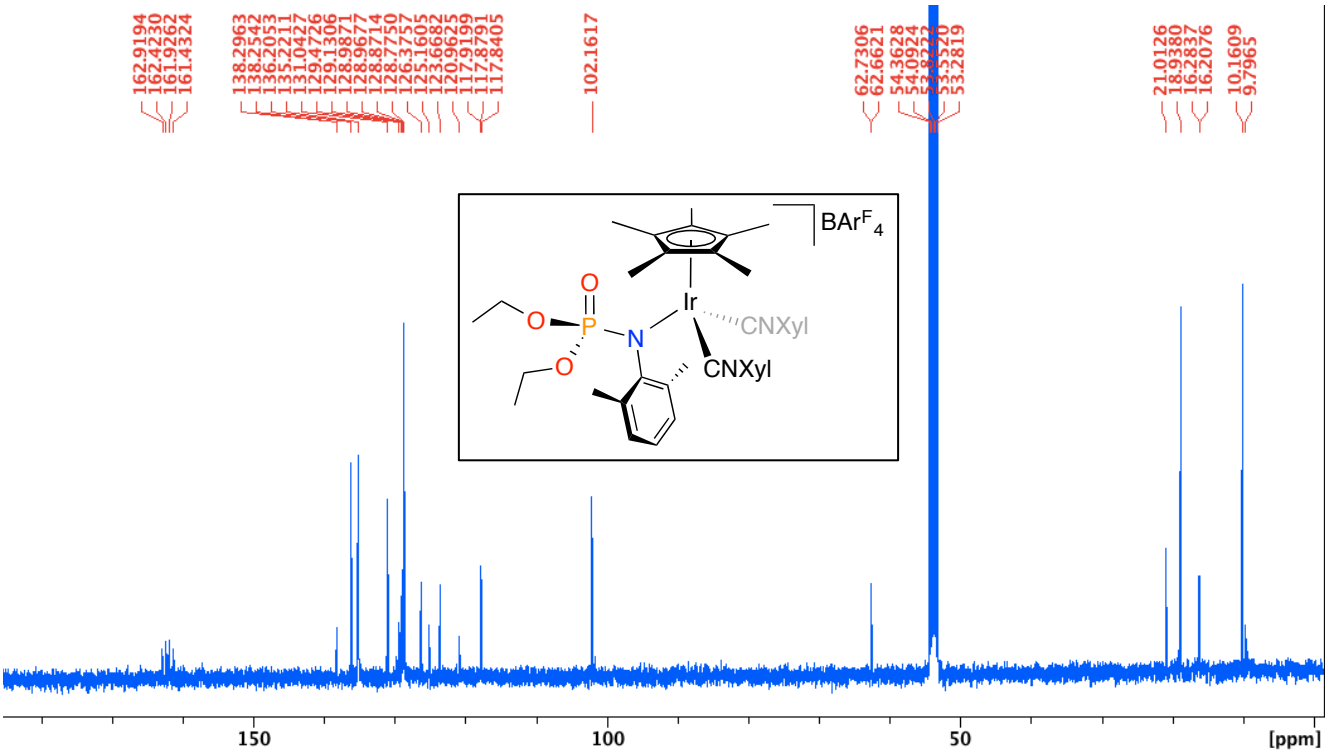

Figure S15. [4][BAr$^F_4$], ESI(+)-MS

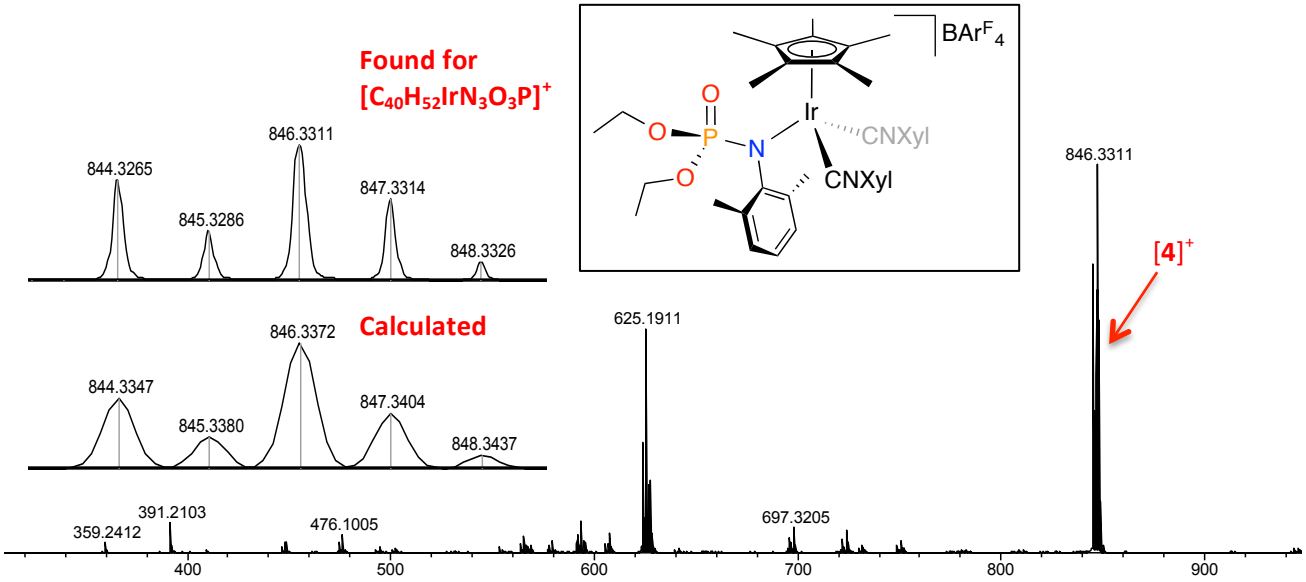

Figure S16. [7][BAr$^F_4$], ^{1}H NMR, CD_2Cl_2, 500 MHz, 298 K, showing signal broadening upon addition of excess MeCN

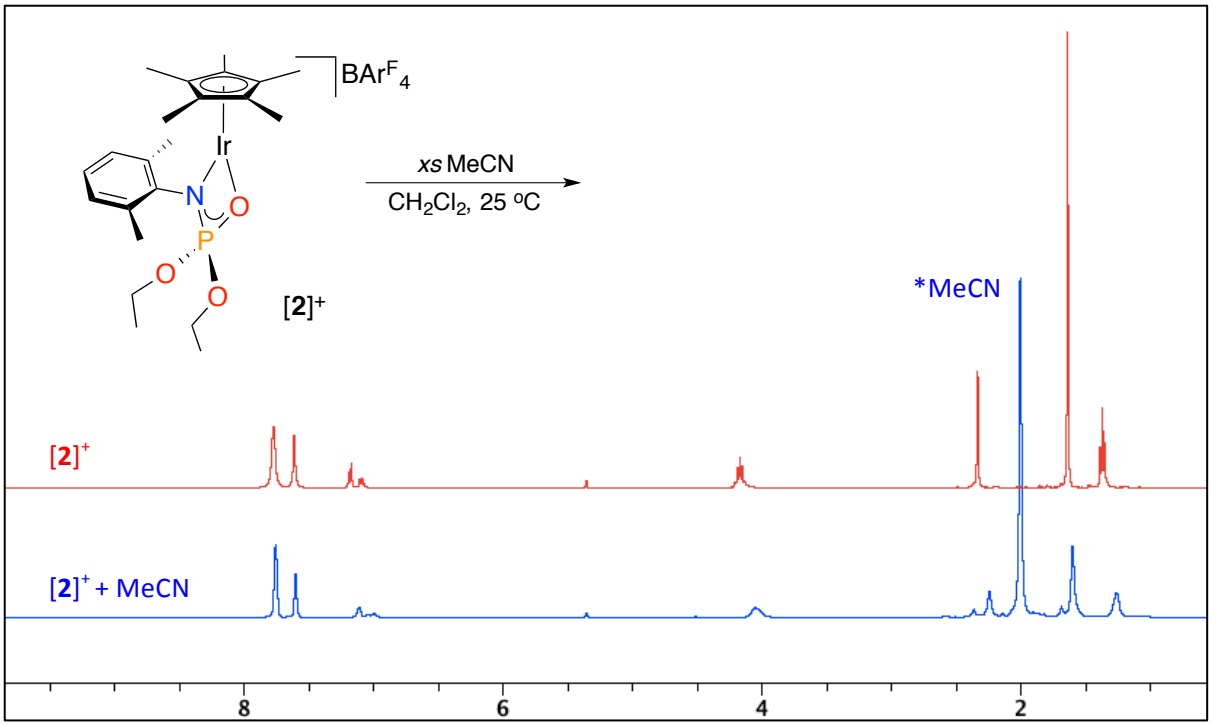

Figure S17. [7][BAr$^F_4$], VT-^{31}P{^{1}H} NMR, CD_2Cl_2, 202.5 MHz, 298 K showing consumption of complex [**2**][**BAr$^F_4$**] and formation of proposed complex [**7**][**BAr$^F_4$**] at low temperature.

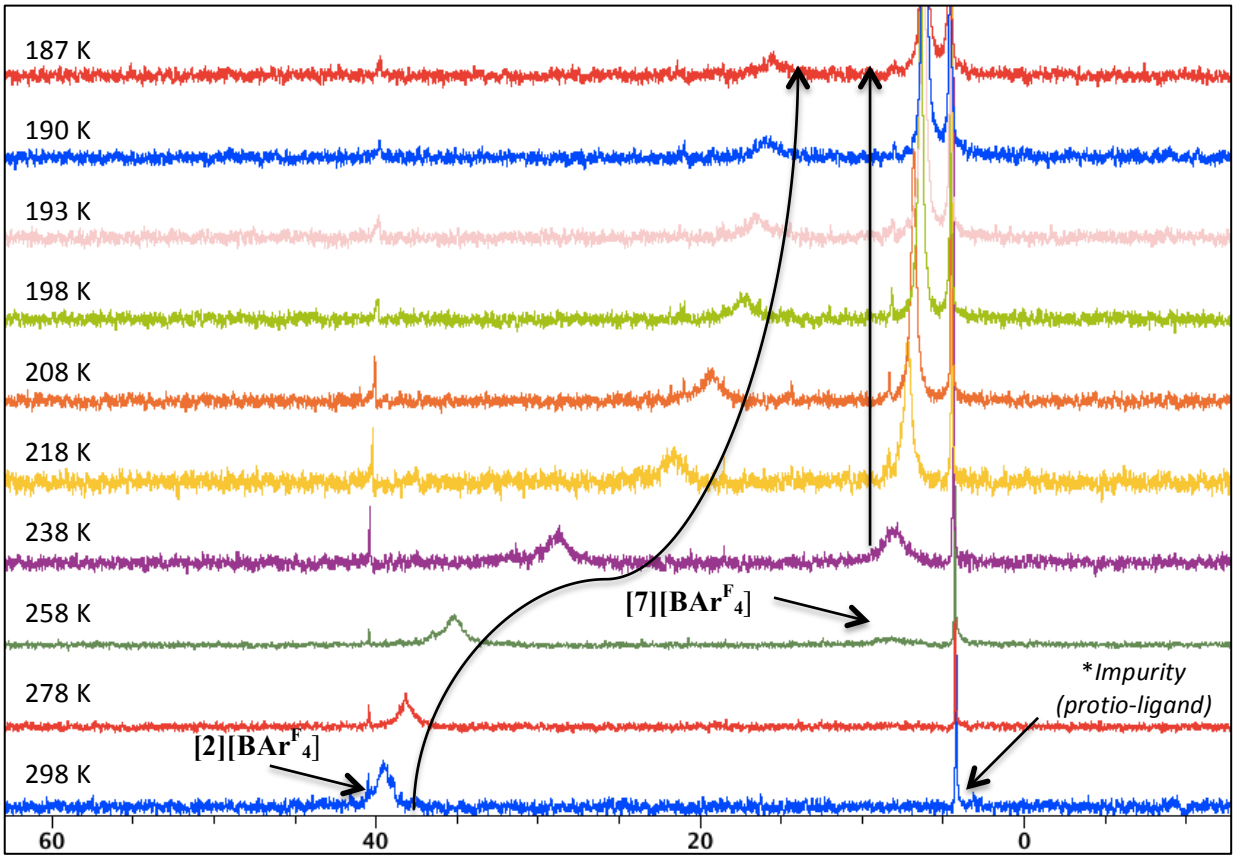

Figure S18. [8][BAr$^F_4$], ^{1}H NMR, CD_2Cl_2, 400 MHz, 298 K

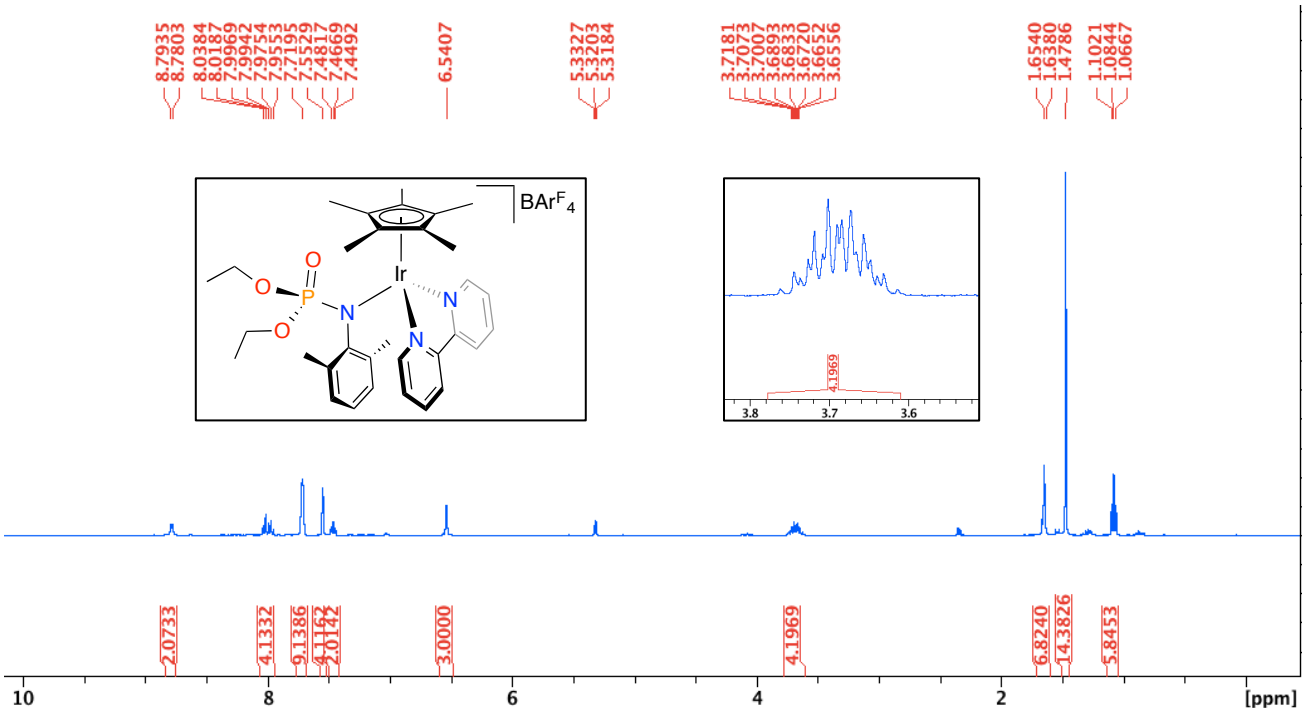

Figure S19. [8][BAr$^F_4$], $^{31}P\{^1H\}$ NMR, CD_2Cl_2, 121 MHz, 298 K

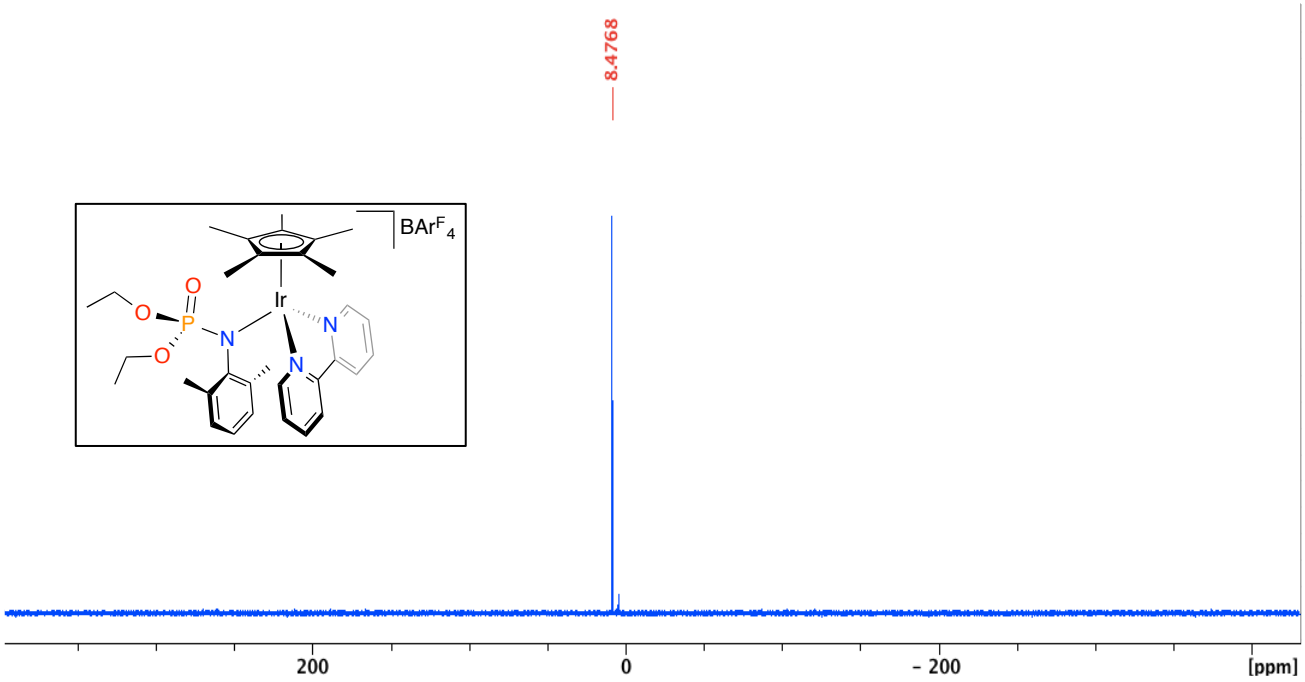

Figure S20. [8][BAr$^F_4$], $^{13}C\{^1H\}$ NMR, CD_2Cl_2, 150 MHz, 298 K

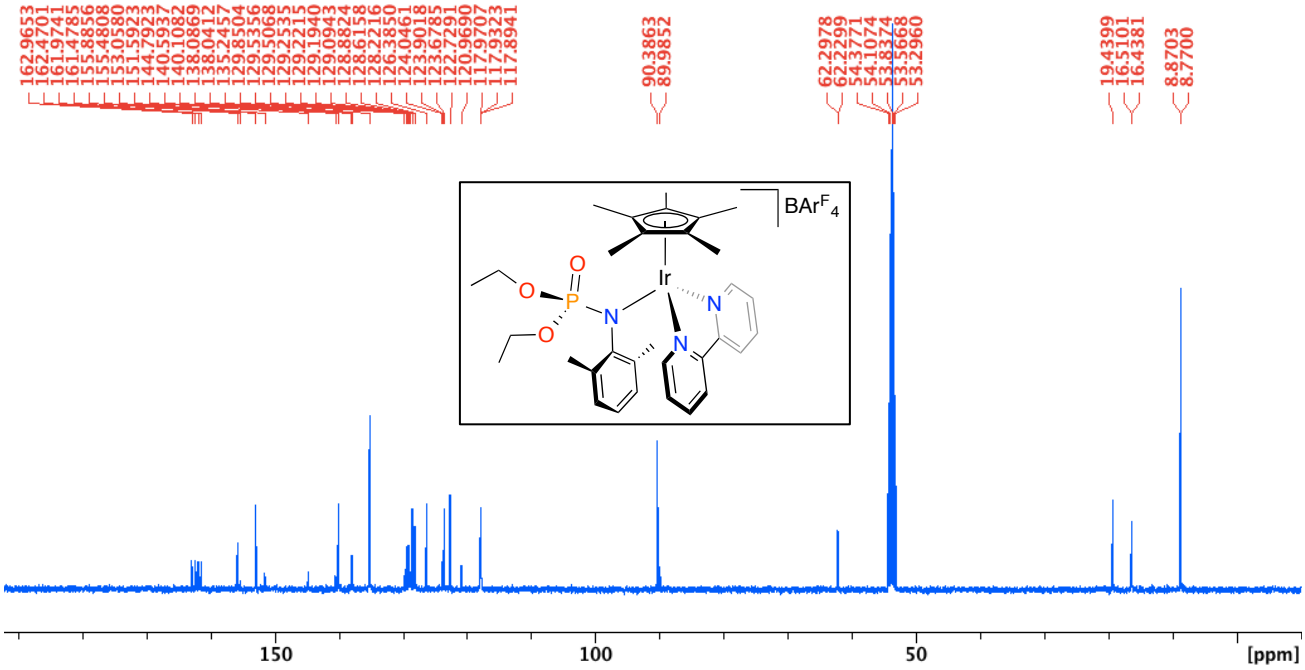

Figure S21. [8][BAr$^F_4$], ESI(+)-MS

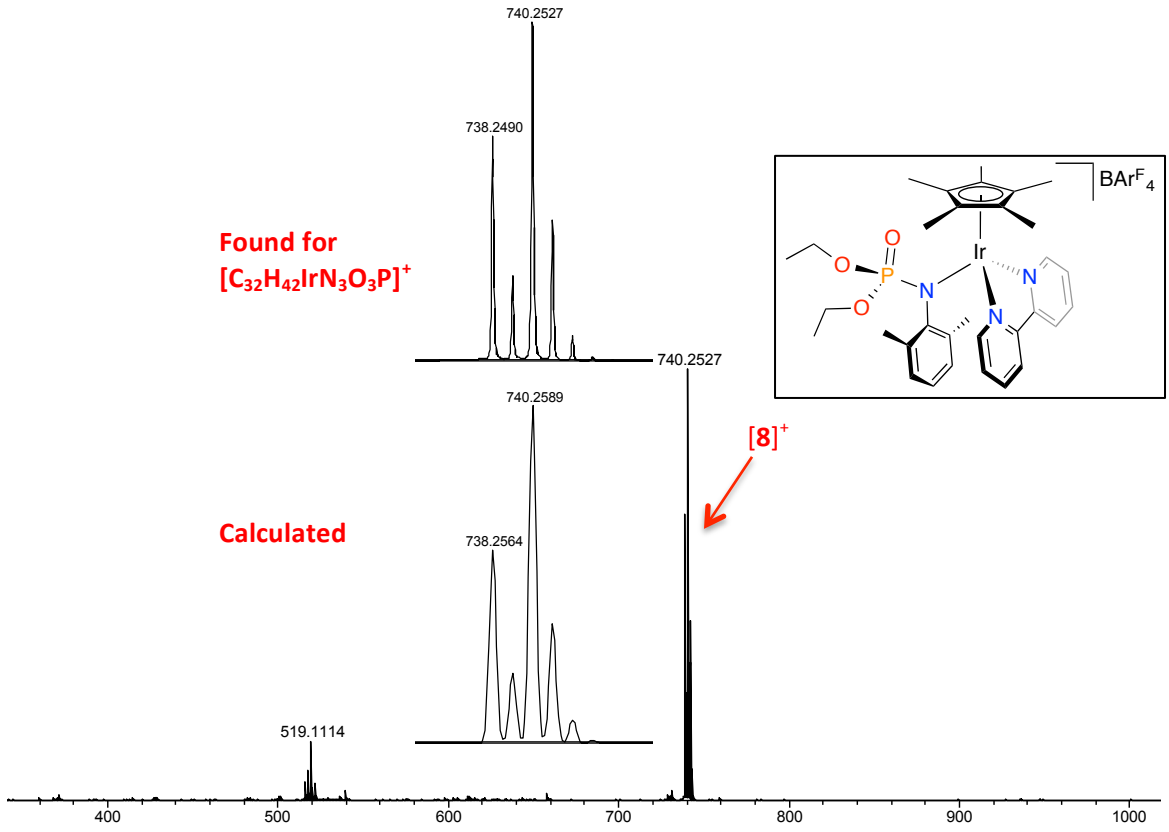

Figure S22. [9][BAr$^F_4$], ^{1}H NMR, $CDCl_3$, 400 MHz, 298 K

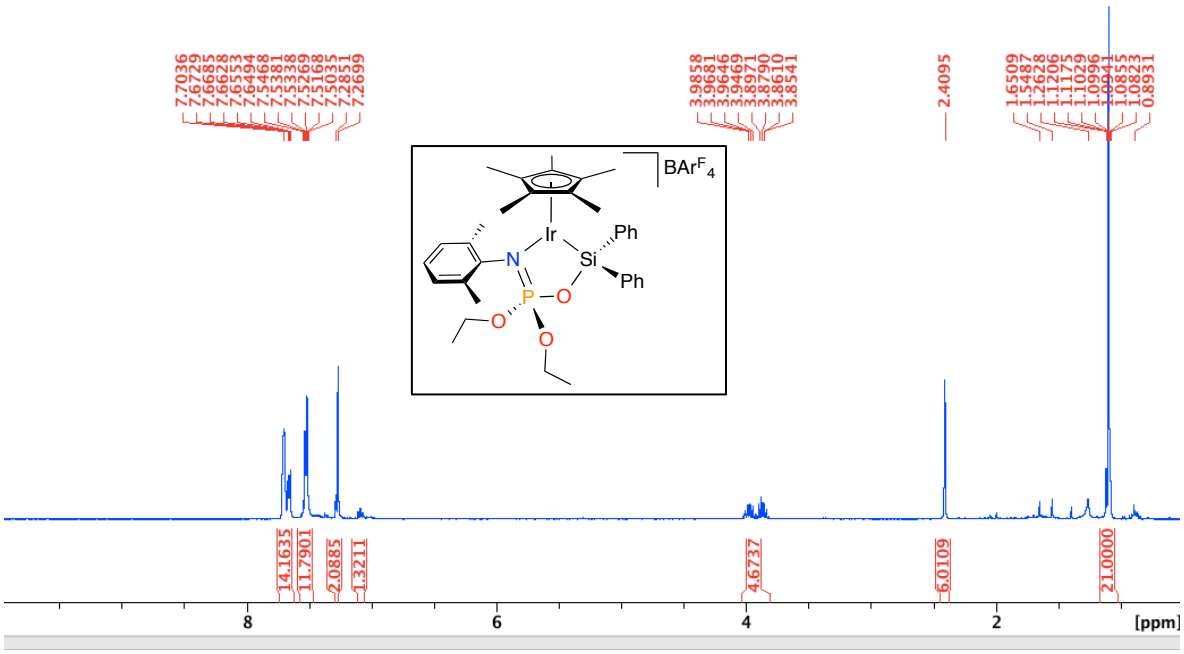

Figure S23. [9][BAr$^F_4$], ^{1}H NMR, $CDCl_3$, 400 MHz, 298 K (expanded baseline)

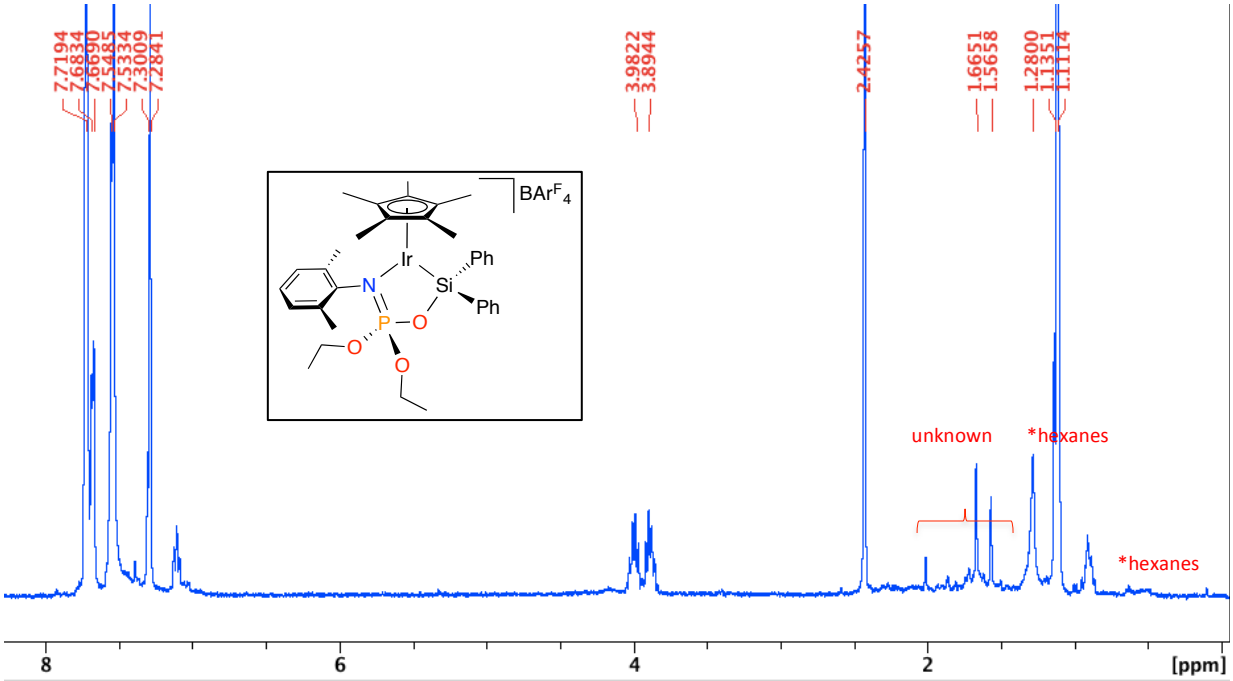

Figure S24. [9][BAr$^F_4$], ^{31}P{^{1}H} NMR, $CDCl_3$, 121 MHz, 298 K

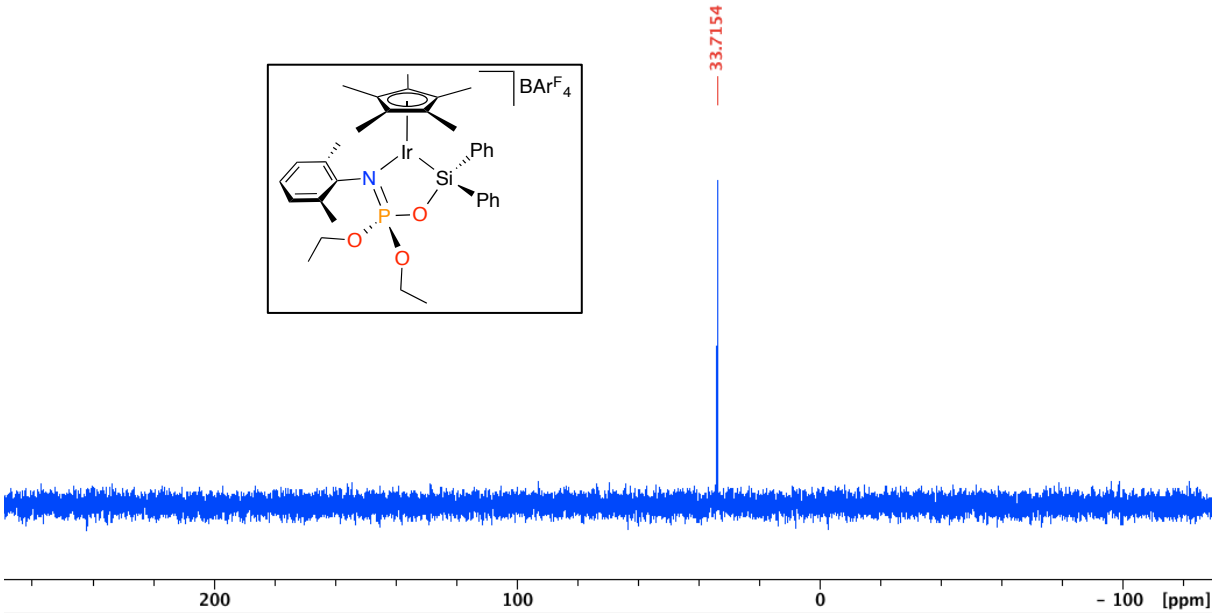

Figure S25. [9][BAr$^F_4$], $^{13}C\{^1H\}$ NMR, $CDCl_3$, 100 MHz, 298 K

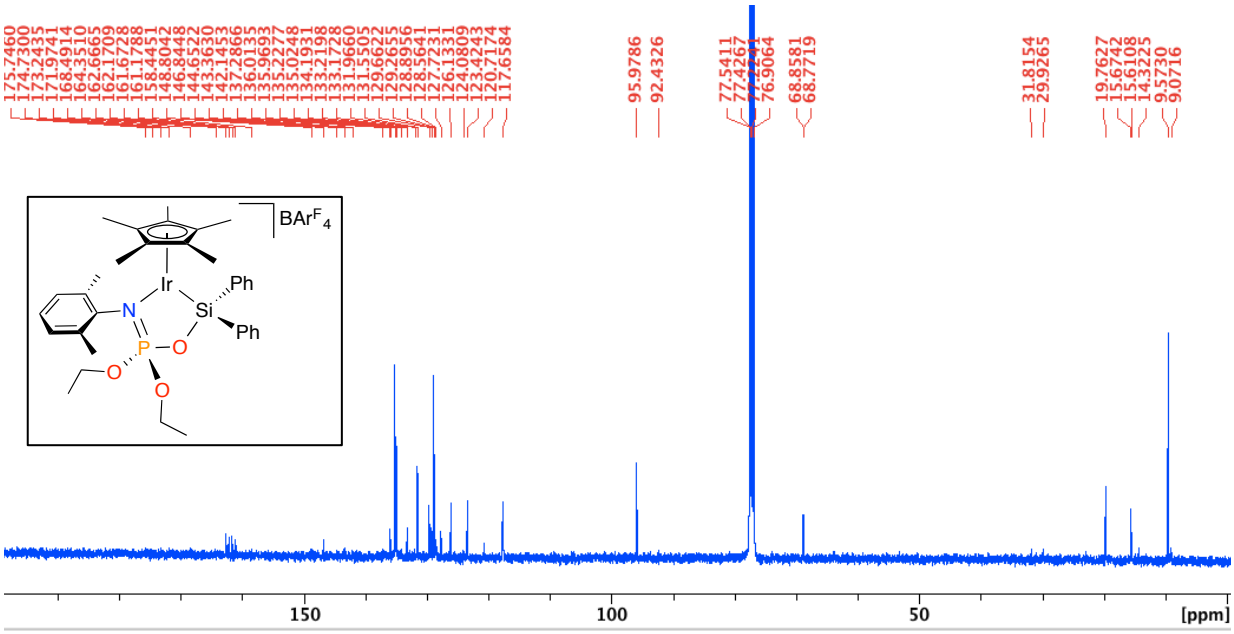

Figure S26. [9][BAr$^F_4$], ^1H-$^{29}Si\{^1H\}$ NMR, $CDCl_3$, 400 MHz (^1H), 298 K (CNST = $J_{Si,H}$ = 10 Hz)

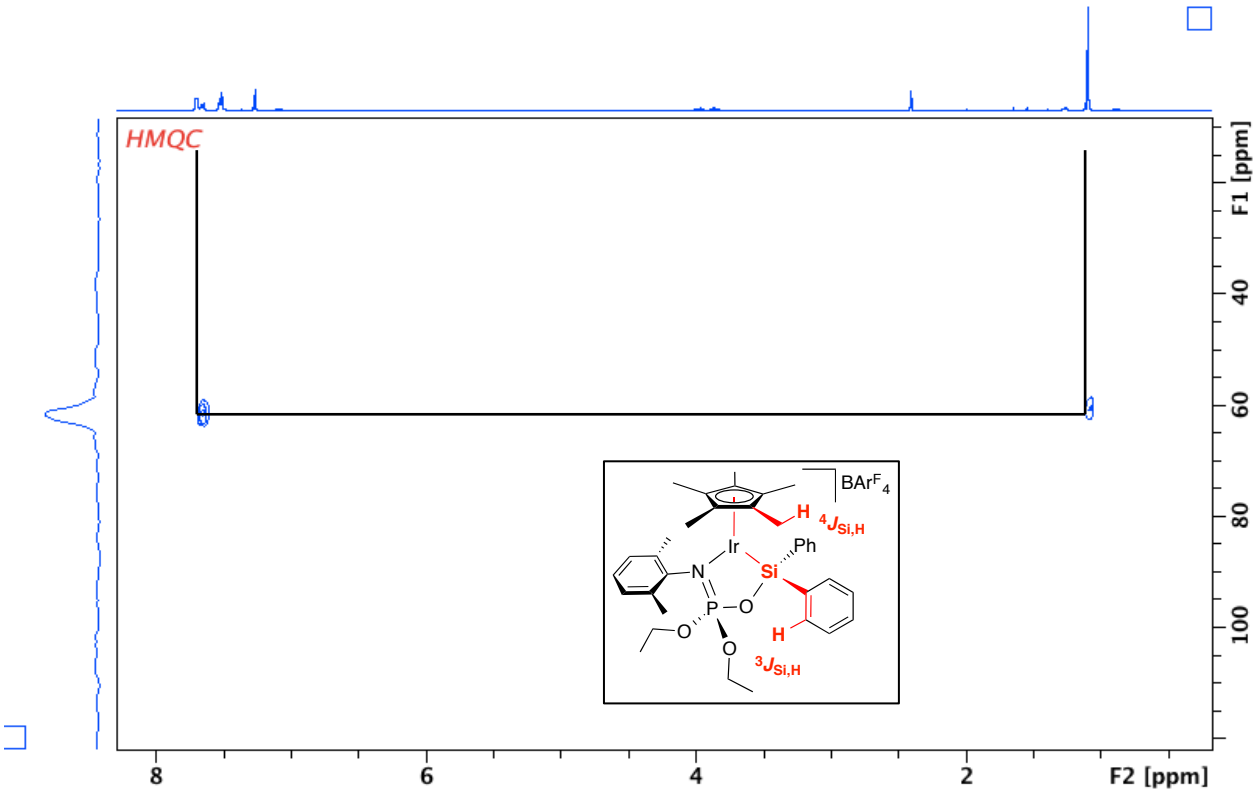

Figure S27. [9][BAr$^F_4$], ESI(+)-MS

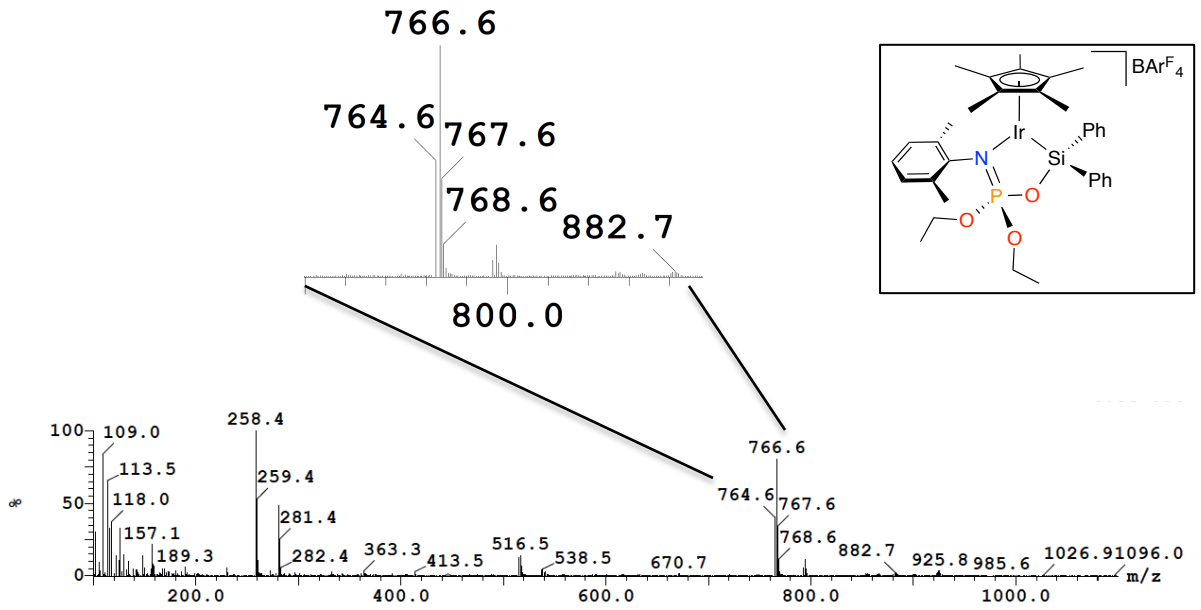

Figure S28. [10][BAr$^F_4$], ^{1}H NMR, CD_2Cl_2, 400 MHz, 298 K

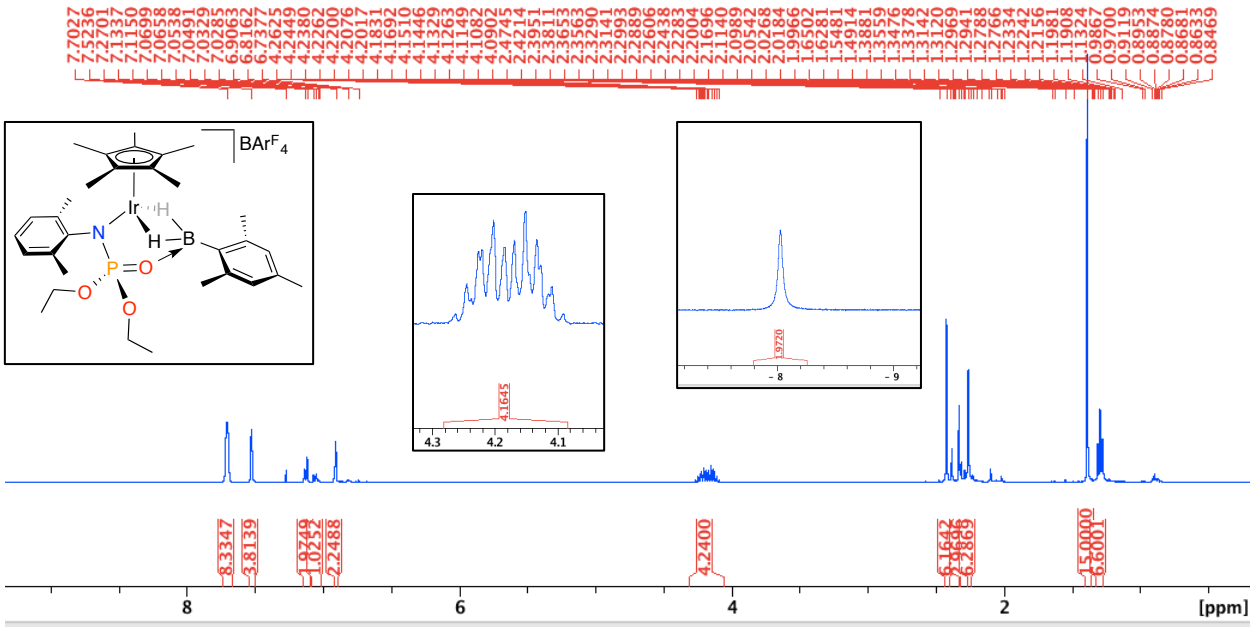

Figure S29. **[10][BAr$^F_4$]**, $^{31}P\{^1H\}$ NMR, CD_2Cl_2, 121 MHz, 298 K

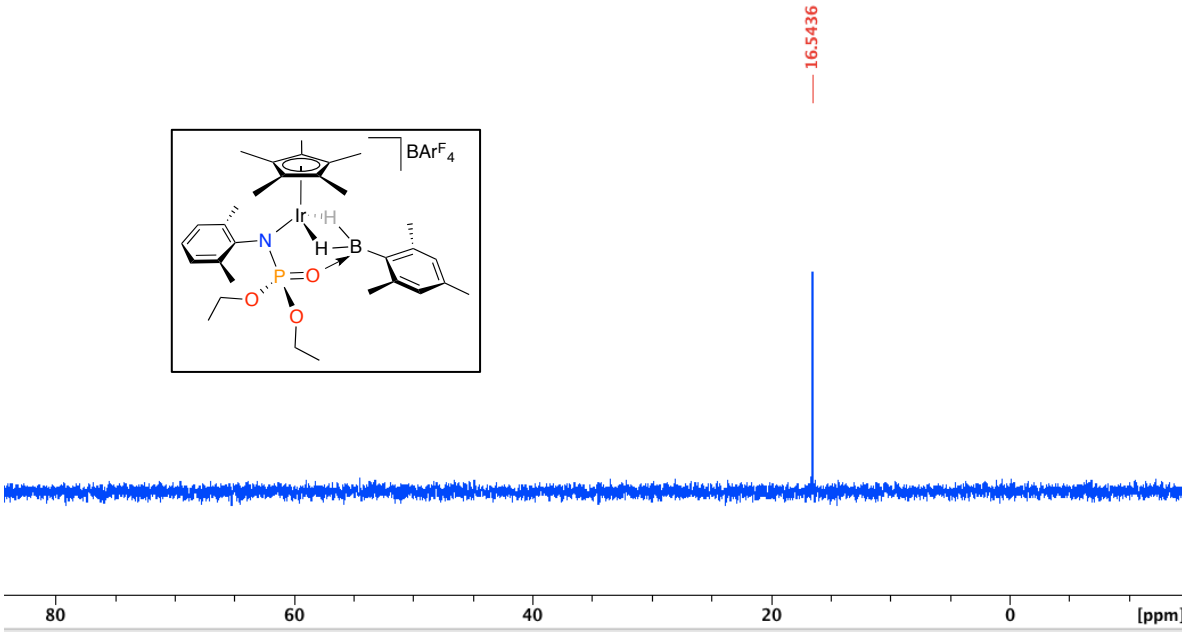

Figure S30. **[10][BAr$^F_4$]**, $^{11}B\{^1H\}$ NMR, CD_2Cl_2, 128.4 MHz, 298 K

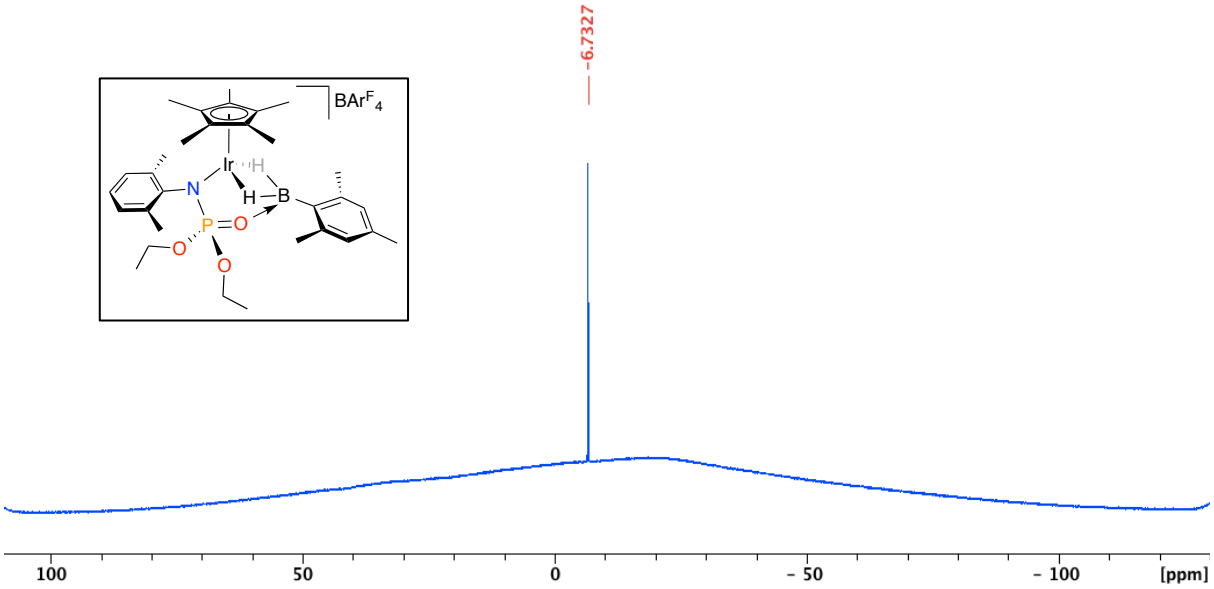

Figure S31. [Cp*Ir(κ^3-*N,H,H*-Xyl(N)P(OBH$_2$Dur)(OEt)$_2$)][BAr$^F{}_4$] (Dur = 2,3,5,6-tetramethylphenyl), ^{11}B{^{1}H} NMR, CD_2Cl_2, 128.4 MHz, 298 K

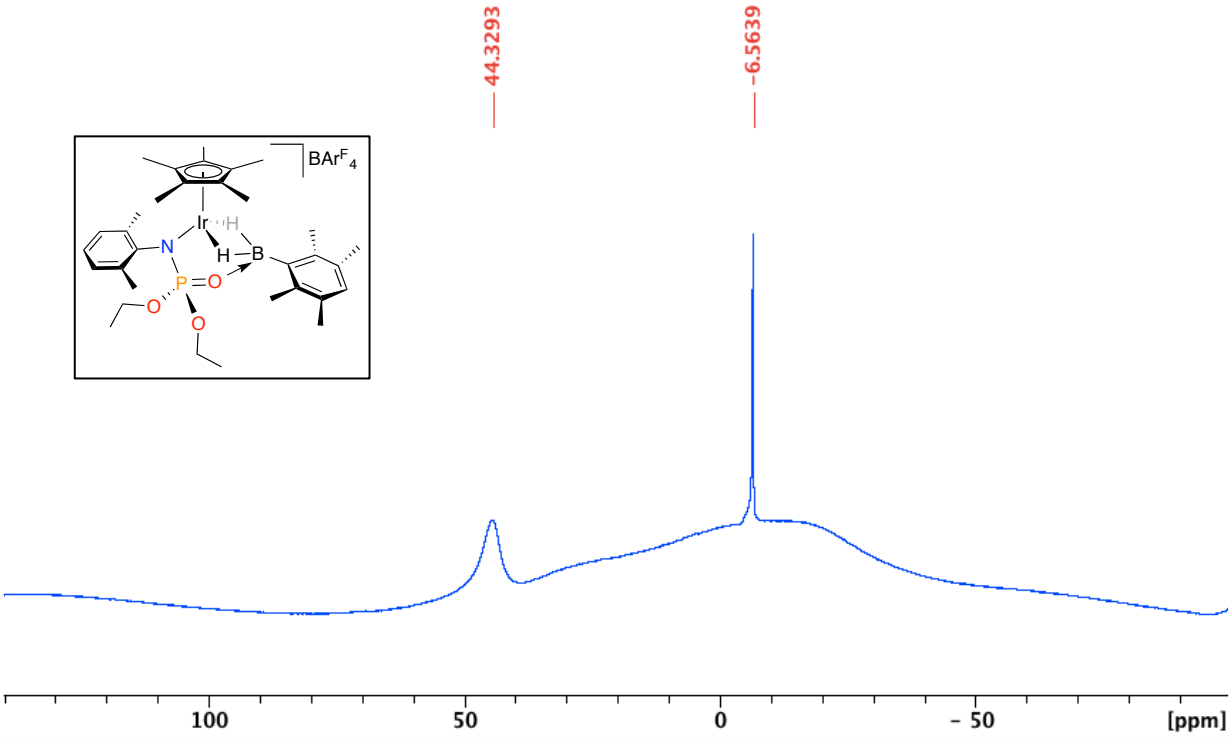

Figure S32. **[10][BAr$^F{}_4$]**, ^{13}C{^{1}H} NMR, CD_2Cl_2, 100 MHz, 298 K

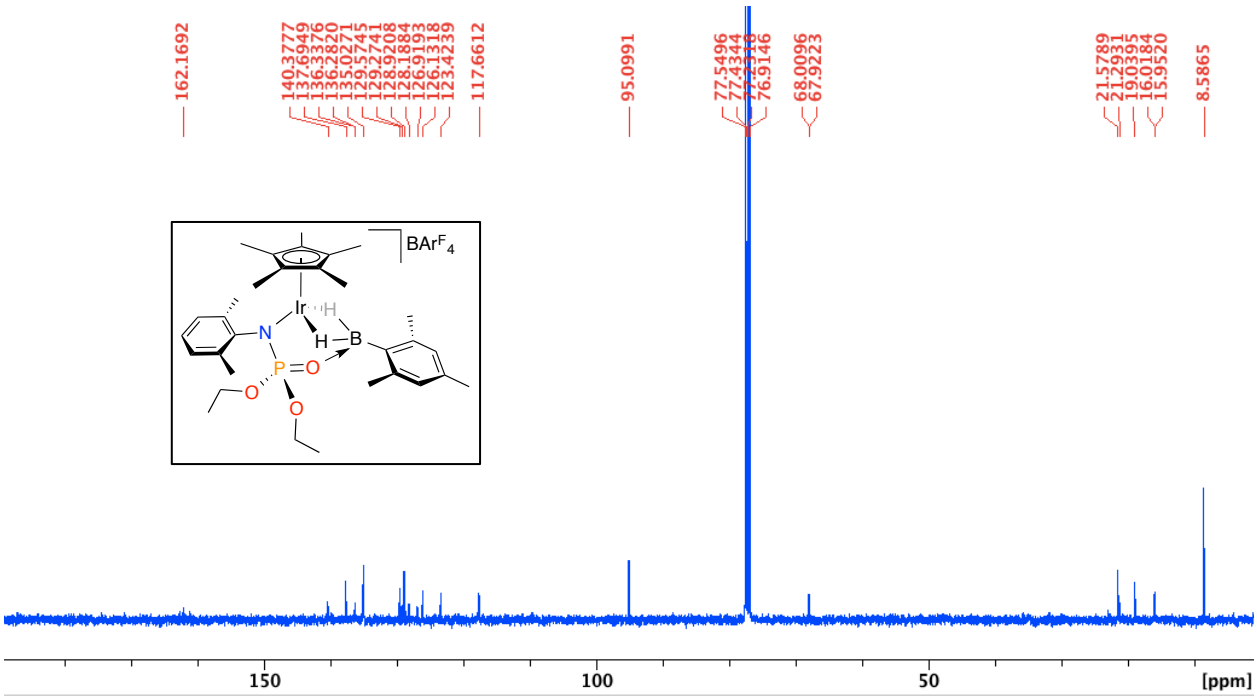

Figure S33. [10][BAr$^F_4$], ESI(+)-MS

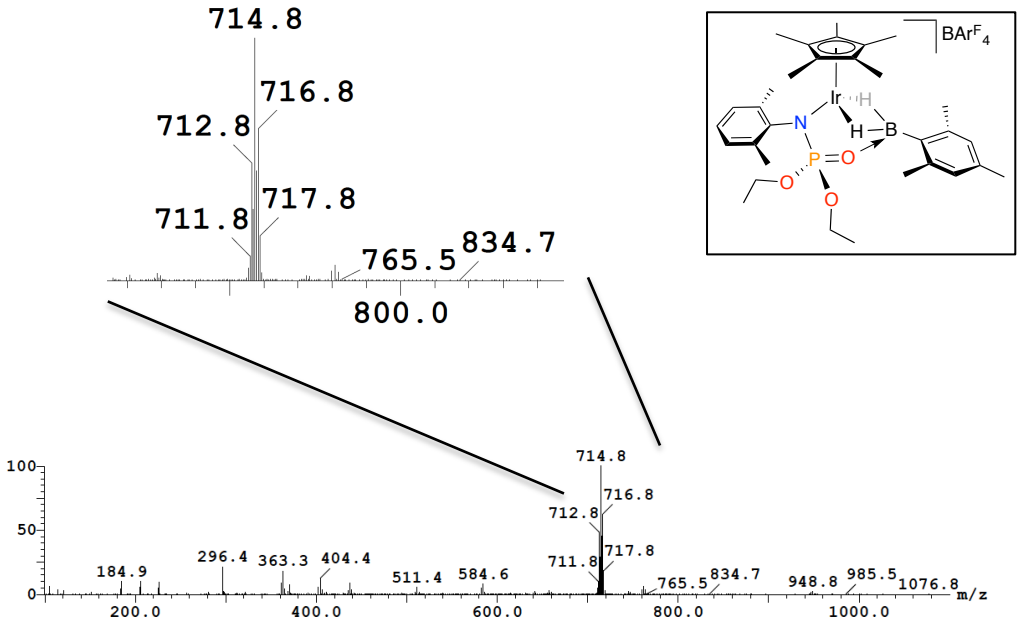

Figure S34. [11][BAr$^F_4$], ^{1}H NMR, $CDCl_3$, 400 MHz, 298 K

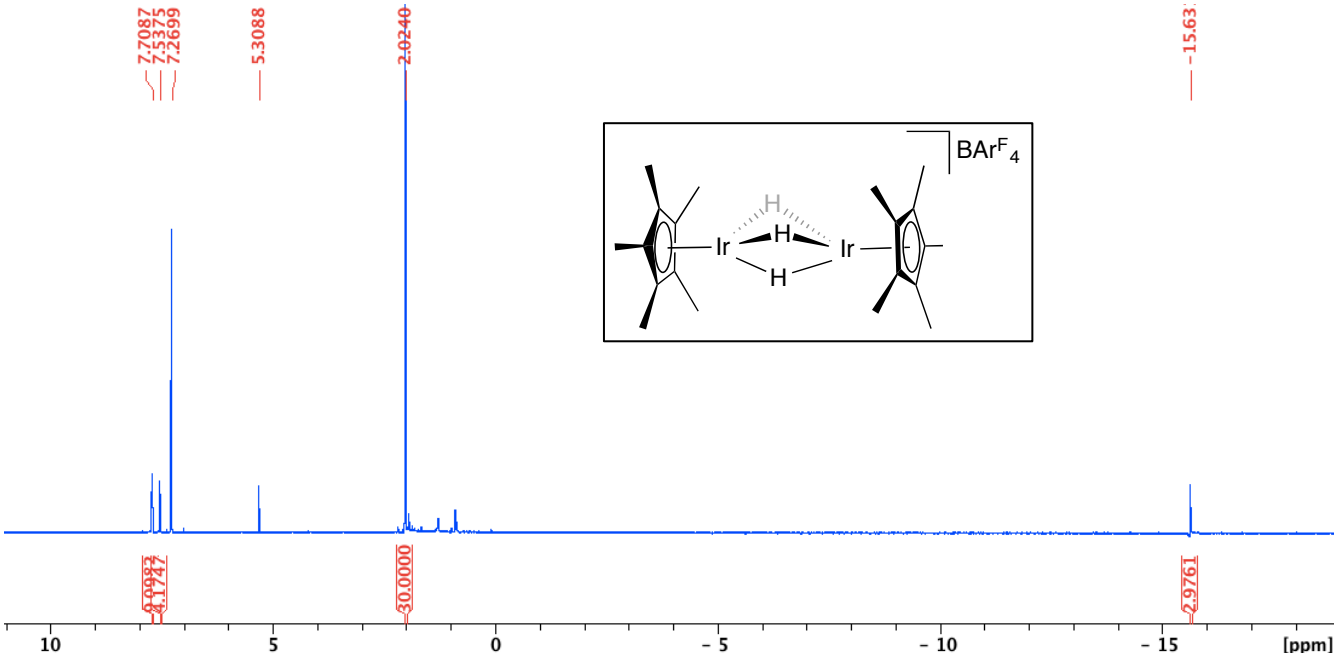

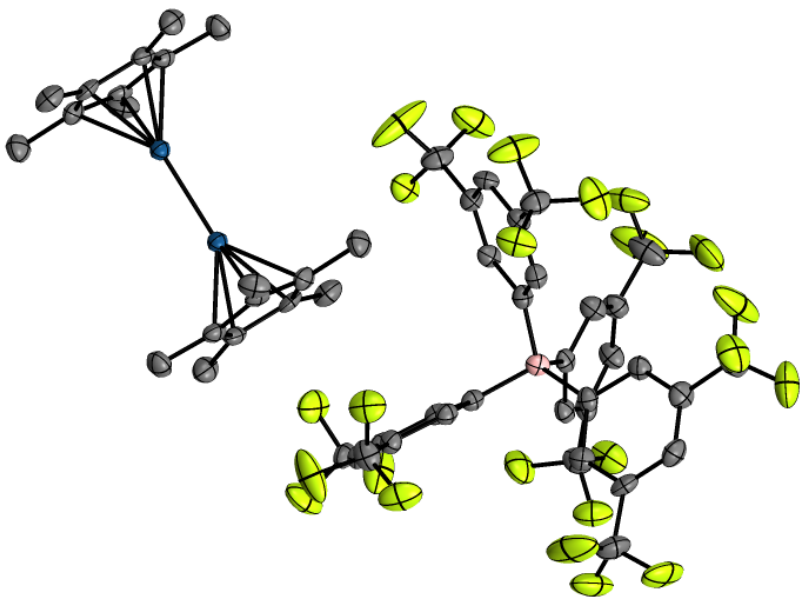

Figure S35. ORTEP depiction of the solid-state molecular structure of $[Cp^*_2Ir_2(\mu\text{-}H)_3][BAr^F_4]$ [**11**]$[BAr^F_4]$ (displacement ellipsoids are shown at the 50% probability, hydrogens omitted for clarity).

Table S1. Crystallographic data for **[2]**[$BAr^{Cl2}{}_4$] and **[3]**[$BAr^{F}{}_4$]

Compound	**[2]**[$BAr^{Cl2}{}_4$]	**[3]**[$BAr^{F}{}_4$]
Empirical formula	$C_{46}H_{46}BCl_8IrNO_3P$	$C_{65.04}H_{66.09}BCl_2F_{24}IrN_3O_{3.02}P$
Formula weight	1178.50	1698.91
Temperature/K	150	90
Crystal system	Monoclinic	Orthorhombic
Space group	P 2_1/n	Pbca
a/Å	13.3463(1)	17.9224(10)
b/Å	20.8617(2)	24.6821(12)
c/Å	17.8625(2)	31.8660(16)
α/°	90	90
β/°	94.8267(4)	90
γ/°	90	90
V/Å^3	4955.76(8)	14096.3(13)
Z	4	8
ρ/ g/cm^{-3}	1.579	1.601
μ/ mm^{-1}	3.198	2.103
F(000)	2344.0	6788.0
Crystal size/ mm^3	0.16 × 0.14 × 0.04	0.41 × 0.21 × 0.14
Radiation	Mo Kα (λ = 0.71073)	MoKα (λ = 0.71073)
2θ range for datacollection/°	10.242 to 54.988	3.086 to 52.9
Index ranges	$-17 \leq h \leq 17$, $-27 \leq k \leq 23$, $-23 \leq l \leq 23$	$-22 \leq h \leq 22$, $-30 \leq k \leq 30$, $-39 \leq l \leq 39$
Independent reflections	11286 [R_{int} = 0.040, R_{sigma} = N/A]	14475 [R_{int} = 0.1366, R_{sigma} = 0.0817]
Data/restraints/parameters	11286/0/550	14475/970/976
Goodness-of-fit on F^2	0.915	1.028
R [I>=2θ (I)] (R1, wR2)	(0.0355, 0.0689)	(0.0499, 0.0939)
R (all data) (R1, wR2)	(0.0642, 0.0762)	(0.0991, 0.1113)
Largest diff. peak/hole / (e Å^{-3})	(2.74, -1.64)	(1.45/-1.33)

$R1 = \Sigma \, ||F_o|-|F_c|| \, / \, \Sigma \, |F_o|$; $wR2 = [\Sigma(w(F_o^2 - F_c^2)^2) \, / \, \Sigma \, w(F_o^2)^2]^{1/2}$

Table S2 Crystallographic data for **[9]**[BAr^F_4] and **[11]**[BAr^F_4]

Compound	**[9]**[BAr^F_4]	**[11]**[BAr^F_4]
Empirical formula	$C_{66}H_{56}BF_{24}IrNO_3PSi$	$C_{52}H_{42}BF_{24}Ir_2$
Formula weight	1629.18	1518.11
Temperature/K	90.0	150
Crystal system	Triclinic	Triclinic
Space group	P-1	P-1
a/Å	12.3952(19)	10.8290(2)
b/Å	15.021(2)	12.6902(2)
c/Å	18.869(3)	19.9820(4)
α/°	71.324(3)	91.0343(7)
β/°	80.182(3)	97.3543(7)
γ/°	84.966(3)	98.1876(8)
V/Å^3	3277.3(9)	2693.78(9)
Z	2	2
ρ/ g/cm^{-3}	1.651	1.872
μ/ mm^{-1}	2.195	5.054
F(000)	1620.0	1458.0
Crystal size/ mm^3	0.42 × 0.23 × 0.14	0.10 × 0.08 × 0.08
Radiation	MoKα (λ = 0.71073)	Mo Kα (λ = 0.71073)
2θ range for datacollection/°	2.864 to 61.246	10.296 to 55.04
Index ranges	$-17 \le h \le 17$, $-21 \le k \le 19$, $-26 \le l \le 26$	$-14 \le h \le 14$, $-16 \le k \le 16$, $-25 \le l \le 25$
Independent reflections	20042 [R_{int} = 0.0272, R_{sigma} = 0.0263]	12286 [R_{int} = 0.046, R_{sigma} = N/A]
Data/restraints/parameters	20042/927/904	22708/0/547
Goodness-of-fit on F^2	1.103	0.923
R [I>=2θ (I)] (R1, wR2)	(0.0380, 0.0927)	(0.0433, 0.0840)
R (all data) (R1, wR2)	(0.0438, 0.0966)	(0.0778, 0.0944)
Largest diff. peak/hole / (e Å^{-3})	(4.00/-1.34)	(4.01, -4.30)

$R1 = \Sigma \, ||F_o|-|F_c|| \, / \, \Sigma \, |F_o|$; $wR2 = [\Sigma(w(F_o^2 - F_c^2)^2) \, / \, \Sigma \, w(F_o^2)^2]^{1/2}$

Crystallographic details

Data for **[2]**[BAr^{Cl2}_4], **[3]**[BAr^F_4], **[9]**[BAr^F_4], and **[11]**[BAr^F_4] were collected using graphite-monochromated Mo K_α radiation (l=0.71073 Å). CCDC 1061938 (**[2][BAr^{Cl2}_4]**), 1403652 (**[3][BAr^F_4]**), 1403651 (**[9][BAr^F_4]**), and 1061937 (**[11][BAr^F_4]**) contains the supplementary crystallographic data for this paper. These data can be obtained free of charge from The Cambridge Crystallographic Data Centre *via* www.ccdc.cam.ac.uk/data_request/cif. For **[3]**[BAr^F_4], **[9]**[BAr^F_4], and **[11]**[BAr^F_4] rotational disorder of the anion CF_3 groups treated by modelling the fluorine atoms over two sites and restraining their geometry. For **[3]**[BAr^F_4], one of the $P(OCH_2CH_3)$ ligand arms was disordered and modelled over three positions. For **[11]**[BAr^F_4] the hydrogen atoms were found on the Fourier map and refined before adding RIDE restraints. Hydrides bridging the two Ir centres, while implicated by other spectroscopic techniques, could not be reliably located/refined.